Analysing spatio-temporal patterns of the global NO_2-distribution retrieved from GOME satellite observations using a generalized additive model

M. Hayn[1], S. Beirle[2], F.A. Hamprecht[3], U. Platt[4], B.H. Menze[3,5*], T. Wagner[2,*]

[1] {Institut für Mathematik, University of Potsdam, Potsdam, Germany}

[2] {MPI for Chemistry, Mainz, Germany}

[3] {Interdisciplinary Center for Scientific Computing, University of Heidelberg, Heidelberg, Germany}

[4] {Institut für Umweltphysik, University of Heidelberg, Heidelberg, Germany}

[5] {Computer Science and Artificial Intelligence Lab, Massachusetts Institute of Technology, Cambridge/MA, USA}

(* contributed equally)

Correspondence to: Michael Hayn (hayn@math.uni-potsdam.de), Thomas Wagner (thomas.wagner@mpch-mainz.mpg.de)

Abstract

With the increasing availability of observations from different space-borne sensors, the joint analysis of observational data from multiple sources becomes more and more attractive. For such an analysis -- oftentimes with little prior knowledge about local and global interactions between the different observational variables available --an explorative data-driven analysis of the remote sensing data may be of particular relevance.

In the present work we used generalized additive models (GAM) in this task, in an exemplary study of spatio-temporal patterns in the tropospheric NO_2-distribution derived from GOME satellite observations (1996 to 2001) at global scale. We modelled different temporal trends in the time series of the observed NO_2, but focused on identifying correlations between NO_2 and local wind fields. Here, our nonparametric modelling approach had several advantages over standard parametric models: While the model-based analysis allowed to test predefined hypotheses (assuming, for example, sinusoidal seasonal trends) only, the GAM allowed to learn functional relations between different observational variables directly from the data. This was of particular interest in the present task, as little was known about relations between the observed NO_2 distribution and transport processes by local wind fields, and the formulation of general functional relationships to be tested remained difficult.

We found the observed temporal trends – weekly, seasonal and linear changes – to be in overall good agreement with previous studies and alternative ways of data analysis. However, NO_2 observations showed to be affected by wind-dominated processes over several areas, world wide. Here we were able to estimate the extent of areas affected by specific NO_2 emission sources, and to highlight likely atmospheric transport pathways. Overall, using a nonparametric model provided favourable means for a rapid inspection of this large spatio-temporal data set,with less bias than parametric approaches, and allowing to visualize dynamical processes of the NO_2 distribution at a global scale.

1 Introduction

Nitrogen oxides – NO and NO_2, often referred to as NO_x – belong to the most important atmospheric pollutants. NO_2 is poisonous by inhalation (World Health Organization, 2003 and Elsayed, 1994) and NO_x plays an important role in the atmospheric ozone budget (Jacob, 1999 and Seinfeld et al., 1997). NO_x is influencing chemical and biological processes both locally (Uno et al., 1996 and Wakamatsu et al., 1998) and globally (Stohl et al., 2003 and Wenig et al., 2003), and its occurrence is closely related to human activities. Tropospheric NO_x is a major contributor to tropospheric ozone smog in urban areas, and even at global scale a disproportionally high amount of the NO_x originates from anthropogenic sources (Olivier et al., 1990 and Seinfeld et al., 1997).

With space-borne instruments, such as the Global Ozone Monitoring Experiment (GOME), global time series of NO_2 and other tropospheric trace gases become increasingly available, with a considerable resolution both in time and space (ESA, 1995; Burrows et al., 1999; Bovensmann et al., 1999 and Wagner et al., 2008, Leue et al., 2001; Richter et al., 2002; Martin et al., 2002; Beirle et al., 2003; Beirle, 2004a,b and Boersma et al., 2004). Also, with an increasing amount of observations from other space-borne sensors and high level products derived from them, such as e.g. global 3-dimensional wind fields, the joint analysis of observational data from multiple sources becomes more and more attractive. Here, with little prior knowledge about local and global interactions between the different observational variables available, an explorative data-driven analysis of the remote sensing data may be of particular relevance.

A number of earlier studies focused on the global distribution of different temporal patterns in the NO_2 dynamics. Examples are the weekly cycle found to correlate well with anthropogenic sources (Beirle et al., 2003), the analysis of long term trends (Richter et al., 2005) and multi-component analyses (van der A et al., 2006 and van der A et al., 2008). All these studies used parametric models for the seasonal variation of the temporal trends and ad hoc extensions, e.g. averaging the residual over monthly windows [Beirle et al., 2004b].

In the present study we used a generalized additive model (GAM) (Hastie et al., 1986 and Wood, 2006), which allows to include different components: a parametric linear trend, non-

parametric annual and weekly cycles, and a term for the local wind fields. We chose GAM for two different purposes:

- First, to test the data for temporal trends which are more complex than the parametric formulations used so far to study global trends of the NO_2 distribution – similar to (Brillinger, 1994; Smith et al., 1999; Dominici et al., 2002; Aldrin et al., 2005; Kim et al., 2005 and Stige et al., 2006).
- Second, to model the relation between temporal dynamics of the observed NO_2 and external observational variables, with as little assumptions as possible. This allows us to consider local wind fields in the analysis of the temporal behaviour of the trace gas at a global level – to the best of our knowledge for the first time – and to uncouple local generation and transport of the observed NO_2 distributions.

The influence of this wind component is particularly high close to strong and continuous point sources like power plants or individual cities. Such regions are characterized by strong fluctuations of the tropospheric NO_2 concentration which can be easily identified e.g. by forming the ratio of the standard deviation and the median of the time series of the integrated tropospheric NO_2 concentration. High values of this ratio are e.g. found close to Hongkong and Johannesburg (see Fig. 1) and we will focus on those examples to understand the contribution of local transport processes to the observed NO_2 distributions.

In the following we describe the data used (Section 2) and the GAM adapted to our task (Section 3). We present global maps of spatial and temporal trends from the application of the model to the GOME data, and discuss the influence of the local wind field on the NO_2 trace gas dynamics observed (Section 4).

2 GOME instrument and data retrieval

The GOME instrument is one of several instruments aboard the European research satellite ERS-2 [*European Space Agency* (*ESA),* 1995; Burrows et al., 1999]. It consists of a set of four spectrometers that simultaneously measure sunlight scattered and reflected from the Earth's atmosphere and ground in total of 4096 spectral channels covering the wavelength range between 240 and 790 nm with moderate spectral resolutions. While GOME was primarily designed for the observation of the ozone layer, in addition, many other trace gases can be also analysed from the spectra, several of them for the first time from space [e.g. Burrows et al., 1999]. The satellite operates in a nearly polar, sun-synchronous orbit at an altitude of 780 km with an equator crossing time at approximately 10:30 local time. While the satellite orbits the earth in an almost north-south direction, the GOME instrument scans the surface of earth in the perpendicular east-west direction. During one scan, three individual ground pixels are observed, each covering an area of 320 km east to west by 40 km north to south. They lie side by side: a western, a center, and an eastern pixel. The Earth's surface is totally covered within 3 days (poleward from about 70° latitude within 1 day). During this three day orbital repetition pattern, the local equator crossing time varies by about □35min. Over the considered period (1996-2001), these patterns of equator crossing times stayed constant.

In the raw spectra taken by the satellite, the NO_2 absorption around 430 nm is analysed by differential optical absorption spectroscopy (DOAS, see Platt and Stutz, 2008; Wagner et al., 2008). Besides the NO_2 cross section also those for O_3, H_2O, and the oxygen dimer O_4, as well as a Ring spectrum are included in the analysis (for details of the spectral analysis see also Leue et al., 2001 and Beirle, 2004a). Output of the DOAS analysis is the NO_2 slant column density (SCD), the NO_2 concentration integrated along the atmospheric absorption path.

The vertical column density (VCD), the amount of molecules in a vertical column, was calculated from the SCD by means of modeled Air Mass Factor (AMF) (Solomon et al., 1987 and Leue et al., 2001). For simplicity, an AMF for a purely stratospheric NO_2 concentration profile was used (see also Leue et al., 2001 and Velders et al., 2001). To obtain the tropospheric NO_2 VCD from the total VCD, the stratospheric part of the total VCD has to be subtracted. In this study the stratospheric NO_2 VCD was estimated over a reference sector over the Pacific and then subtracted from the total NO_2 VCD measured at any location at the

same latitude (see also Richter et al., 2002). The difference was used as the final estimate of the tropospheric NO_2 vertical column density, referred to as NO_2 TVCD in the following. It should be noted that by applying such simple stratospheric corrections, components of the annual cycle of the stratosphere might be artificially transferred to the estimated tropospheric NO_2 TVCD, especially in the presence of longitudinal gradients of the stratospheric NO_2 distributions. Moreover, the use of a stratospheric air mass factors may also have lead to an under-estimation of the NO_2 TVCD, by a factor between 2 and 4 (Leue et al., 2001 and Velders et al., 2001) which is dependant on cloud cover. To reduce this bias, we confined ourselves to use observations with an effective cloud fraction of 0.3 at maximum. The information about the cloud fractions was also obtained from GOME observations using the HICRU algorithm (Grzegorski et al., 2006).

The data used in the following are from the period beginning on 17th January 1996 and ending on 31st December 2001. The observational data was re-sampled at a spatial resolution of 0.5 × 0.5 degrees of latitude and longitude, respectively, with 0.5 being the approximate north-south range of the scan. This is a reasonable compromise between obtaining high resolution maps and working with at a resolution which can be supported by the satellite data. In addition to the GOME NO_2 measurements, freely available wind data of the European Center for Medium range Weather Forecasting (ECMWF) were used (Kållberg, 2004). The resolution of the wind data is 2.5 × 2.5 degree in latitude and longitude. They are temporally sampled in steps of 6 hours (0:00, 6:00, 12:00, 18:00 UTC). Since the satellite crosses the equator at approximately 10:30 local time each orbit, depending on the longitude, the times of the satellite observations and of the modeled data can deviate more or less. We reduced these differences in the time matching by using mean wind speeds averaged over the last 24 hours

3 The Generalized Additive Model

The Generalized Additive Model (GAM) provides a general statistical framework to model the interaction between a specific feature of interest Y and a set of (potentially) explanatory variables X. The methodology behind the GAM follows a data-driven, non-parametric approach and has greater flexibility than the traditional parametric modeling. It has two desirable features in the exploration of large, unstructured data sets: First, a GAM is able to identify those variables x_i in X that are relevant to Y even in a large set of potential candidates. Second, a GAM does not require to define the structural relationship between Y and X right from the outset, but is able to "learn" it from the data, individually for each variable x_i. Hence, their use might be indicated when no prior knowledge about the this relationship is available, and one would like the data to 'suggest' the appropriate functional form; or, when the functional form is expected to be complex – with non-linearities or threshold effects – and cannot easily be represented in a parametric model. In the analysis of the global distribution of NO_2 – our modeled observable Y – we were interested in characterizing the structural relationship between NO_2 and the signal of selected relevant features x_i – representing temporal cycles of predefined length, or the aforementioned wind fields.

3.1 Learning the structural relationship

For each location we had a time series of T measurements of Y available – i.e. a set of approximately 300-700 observations of NO_2 at each location on our global map in the time from 1996 to 2001 – which can be represented by a vector $\mathbf{y}$ of length T, i.e. with $\mathbf{y} \in \mathbf{R}^T$. Variations in the number of available observation resulted from cloud cover and the spatially varying observational coverage with the higher latitudes being more frequently visited by the satellite than equatorial regions. We assume that the measurement $\mathbf{y}$ arises from a true value $\boldsymbol{\eta} \in \mathbf{R}^T$, superposed by a measurement error $\boldsymbol{\varepsilon} \in \mathbf{R}^T$, with $\mathbf{y} = \boldsymbol{\eta} + \boldsymbol{\varepsilon}$. For simplicity we assume ε to be normally distributed for NO_2, although the GAM potentially allows to use different distributional models for ε – for example a binomial distribution in a binary detection task, or a Poisson distribution when measuring rare events (in accordance with Generalized Linear Models (McCullagh et al., 1989)). The additive model assumption requires the true value η of an observation y to result from the superposition of a number of independent processes, represented by functional terms $f_1, \ldots, f_m$ (Hastie et al., 1990). Under these assumptions η can be modeled as

$$\eta = f_1 + \ldots + f_m \quad (1)$$

with the m terms f_j being functions of the n explanatory variables $X=\{x_1,..., x_n\}$ building the observation matrix $\mathbf{X} = [\mathbf{x_1},..., \mathbf{x_n}]$, with $\mathbf{x_i} \in \mathbf{R}^T$. The individual model terms f_j are assumed to be independent: a seasonal model component f_{ann}, for example, would be assumed to be independent from a weekly trend f_{week}, the wind direction f_{wind}, or the amount of rainfall f_{rain}. The functions f_j may depend on one variable x_j only, with $f_j=f_j(x_j)$ as a univariate function, or may depend on several variables, with $f_j=f_j(x_i, x_j, x_k, ...)$. In the present study we confined ourselves to univariate terms, and obtain a model for X and Y with $n = m$.

$$y = f_1(x_1) + \ldots + f_n(x_n) + \varepsilon \quad (2)$$

To estimate the functional form of f_j from the data, the different functional terms f_j can be approximated by univariate splines, which can be fitted to the T observations of (X, Y) under the assumption of a sufficiently "smooth" behaviour of f_j along time:

$$f_j(x_j) = \sum_k \beta_k b_k(x_j) \quad (3)$$

Spline basis $\{b_k\}$ and spline coefficients $\{\beta_k\}$ have either to be predefined (total number k and locations of spline knots, with restrictions on k by the number of observations T), or have to be estimated from the data (spline coefficient $\{\beta_k\}$). To approximate $\mathbf{y_i} = \mathbf{y} - \Sigma_{j=1...n \setminus i} f_j(\mathbf{x_j})$, i.e. the change in y which can be attributed to feature x_i, the function f_i is found as follows:

$$\arg\min_{f_i} \left\| \boldsymbol{y_i} - f_i(\boldsymbol{x_i}) \right\|^2 + \lambda \cdot \int \left\{ f_i''(t) \right\}^2 dt \quad (4)$$

with f_i'' the second derivative of f_i along t, the temporal dimension of the x_i; and λ_i the smoothing parameter governing β_k in (3) for a specific spline representation b. The smoothing parameter λ_i allows to trade the error from over-fitting the noise in the available observations (first term), which results in a rough function f_i, with the bias in model f_i from an unrealistic, overly strong smoothing (second term). It is adjusted to minimize the sum of both fit- and model-error in (4) – the expected prediction error – which can be estimated from the data in a generalized cross-validation (Craven et al., 1979).

Fitting (1) is performed by optimising (4) individually for each model term f_i, and iterating the procedure over all functional models f_i until convergence – a procedure referred to as backfitting (Hastie et al., 1990).

3.2 Model definition and identification of relevant functional terms

Functions f_i of the structural relationship between Y and x_i in (3) can easily be estimated from the data in a nearly automated fashion: Optimizing equation (4) over λ_i according to the cross-validated prediction error allows to generate a large amount of hypotheses on the functional form of f_i, and to test them accordingly (Wood, 2006). The more fundamental definition of the additive model, however, i.e. the identification of the relevant predictors x_i and the specification of the additive terms f_i in equations (1) and (2), will require some amount of user-interaction. Although a concise model (equation (1)) with few explanatory features x_i is preferred over a model with too many predictors – redundant at best, irrelevant or deteriorating at worst – it is possible to start with a model incorporating all available sources of information, and the maximal amount of available observables x_i. After fitting such a model, a study of the functional model terms f_i will allow a qualitative search for irrelevant parameters x_i and a successive optimization of the model (compare figure 3): A functional term f_i which is roughly constant after the optimisation will indicate an irrelevant variable x_i; It can be removed and the set of potential explanatory features X can be reduced successively. An alternative, more quantitative approach in such a recursive elimination of irrelevant terms in equation (1) is provided by an analysis of variance (ANOVA). This procedure compares predictions of a model including a specific term f_i, and predictions of a model without this term, for example also using predictions in a generalized cross-validation. A subsequent statistical test on the significance of the difference between the two distributions allows to score the importance of the tested model term by a p-value (Toutenburg, 2008). If predictions of the complete model are significantly better than the reduced model – measured, for example, by a paired parametric t-test (Toutenburg, 2008), or a non-parametric Cox-Wilcoxon test (Toutenburg, 2008) – the tested model term will be retained. If the reduced model outperforms the complete model, or does not differ significantly from the full model, the model term can be dropped. Providing a quantitative score, the outcome of the test can also be used to compare the relevance of a specific term f_i for the observations (X,Y) at different locations, and, hence, to map the local relevance of the different additive terms f_i of the functional model (equation (1)).

3.3 Application to the spatio-temporal distributions of NO_2

The model used in the following consists of four terms f_i: The annual cycle f_{ann}, the weekly cycle f_{week}, the linear trend $f_{lin}=s*t$ (thus, from a purist point of view one might refer to (1) also as a mixed model), an additive constant μ, and a component f_{wind} modeling the dependence of the NO_2 TVCD y from the wind direction θ .

$$y = \mu + s \cdot t + f_{ann}(t \bmod 365) + f_{week}(t \bmod 7) + f_{wind}(\theta(t)) \qquad (1)$$

The annual cycle f_{ann} is modeled using smoothing splines with periodic boundary conditions:

$$f_{ann}(0) = f_{ann}(365), \quad f'_{ann}(0) = f'_{ann}(365) \qquad (2)$$

As an alternative the annual cycle could be modelled as a discrete function of the month. We could not recognize a striking difference between both models. The weekly cycle f_{week} is a discrete function of the day in the week. Although each of the first three terms is a function of the time, we can assume independence between the explaining variables as we expect different processes to be responsible for changes at the time scales of f_{lin}, f_{week} and f_{ann}. The term f_{wind} is a cyclic spline over the wind direction θ with the additional border conditions:

$$f_{wind}(0) = f_{wind}(2\pi), \quad f'_{wind}(0) = f'_{wind}(2\pi) \qquad (3)$$

Both information about wind direction and wind speed were available from the ECMWF wind data. For reasons of simplicity we confined ourselves to consider the direction of the wind at the surface only. Of course, also the wind speed and its vertical variation can have an influence on the observed NO_2 patterns (although the wind fields at different altitudes are usually highly correlated). As will be shown below, using the wind direction at the surface alone has already a strong influence on the observed NO_2 fields, especially close to strong sources. In future studies using data sets of trace gas concentrations and winds with better spatial resolution and coverage, more properties of the wind field might be included.

It should also be noted that considering the wind speed in addition to the wind direction is not a trivial task, since the components modeled by GAM have a given (additive) form. One solution would be to apply a model with splines in two variables (direction and magnitude of the wind). We leave this as an extension for further studies.

The additive model requires statistical independence of effects modelled by the different model terms. This might not be strictly fulfilled when including both season and wind component which are typically related. A well known example is the winter monsoon and

summer monsoon in south-east Asia. Nevertheless, since wind fields change also on much higher frequencies, it can be expected to have long term changes in (1) absorbed in the f_{ann} term, while the wind direction mainly represents the effects of the short term fluctuations on the NO_2 distribution.

4 Results and Discussion

Results from fitting model (1) to a time series are the different additive functional relationships f_i as shown in figure 2, for four exemplary locations. Here, the first row shows the model coefficients of the different f_i for a location close to Beijing (37.75°N, 114.75°E) representing an example with both a strong annual cycle and a strong linear trend. The second row provides an example for south Australia (22.25°S, 125.25°E), where the seasonal cycle is the only significant component. In the third row results for a location in the North Sea, (54.25°N,7.75°E) are given, with both a dependency to f_{ann} and f_{wind}. In the bottom row result for a location close to Milano (44.75°N,11.25°E) provide an example for a significant linear trend, weekly and seasonal cycle, but a non-significant wind component (here even with a constant function f_{wind})

For a spatial analysis of the model terms features highlighting specific properties of the different f_i, were mapped at a global scale: Figure 3 shows p-values of the different model terms - characterizing the significance for the different components. Amplitudes of the different f_i are shown in figure 4. Figures 5 to 10, map individual coefficients of the weekly cycle, seasonal cycle and the wind term. In the following these maps will be studied in detail. It should be kept in mind, however, that the purpose of these maps is to highlight specific features of the model terms. Patterns identified in the global map are to be checked with the actual functional form of the different f_i.

4.1 Annual cycle

As demonstrated in figure 2, the seasonal cycle can differ significantly from a sinusoid with a period of one year, indicating that the use of a parametric formulation for the seasonal component is more appropriate for the description of the temporal variation of the tropospheric NO_2 VCD. The flexibility of the nonparametric model provides additional information about the annual cycle, such as the temporal distance between minimum and maximum or the number of maxima during one year.

The p-values for the annual cycle (Fig. 3) vary in space on large scales only. This indicates that climatic conditions are expected to have the major impact instead of human sources. In regions with strong influence of biomass burning, lightning activity or soil emissions (Jaegle et al., 2004, van der A et al., 2008), the respective emissions are directly connected to the seasonal variation of temperature, precipitation and convective activity.

In addition, the variation of the atmospheric lifetime as well as wind speed and direction influence the observed tropospheric NO_2 patterns (this is also important for regions with mainly anthropogenic emissions). The "significant annual cycle" in the source free regions over the southern Indian Ocean is probably an artefact caused by the stratospheric correction mentioned in section 2.

The annual component contains information on possible sources and lifetime of NO_2. In figure 5, the month with the maximum NO_2 TVCD is shown. In regions with high anthropogenic emissions the highest values are typically observed in winter time (e.g. in east Asia or the US East coast) indicating high emissions (due to heating) and high atmospheric lifetimes. In some highly polluted regions, however, the highest values are found in other months (see also Fig. 2, North Sea). This might be due to the influence of other parameters like e.g. wind speed and direction.

This indicates that transport processes should be studied separately for summer and winter. Another feature is the winter maximum in the Russian Federation along the Trans-Siberian Railway. The very low temperatures in Northern Russia might cause extremely long lifetimes in those regions during winter.

In other regions of the world the influence of other emission sources like biomass burning, lightning activity and soil emissions lead to pronounced maxima in other months. These findings are in very good agreement with results from (van der A et al. 2008) for most locations. However, in some regions (e.g. the western USA) also systematic differences were found, which are mainly related to the application of the non-parametric description of the annual cycle. An additional reason might be that different periods of time are considered, during which the conditions might have changed.

4.2 Linear Trend

In figure 4, the spatial distribution of linear trends with p-values less than 0.001 for the period 1996-2001 are shown. Significant trends appear mostly in areas with dominant anthropogenic sources. We also obtain low p-values for linear trends which show almost constant behaviour, such as in wide areas of the Indian and Pacific Ocean. It is interesting to note that these areas form the compliment to the areas with significant seasonality.

Significant positive trends appear in China (up to approx. 7×10^{11} [molecules] cm^{-2} day^{-1} = 2.6×10^{14} [molecules] cm^{-2} $year^{-1}$), in the west of USA (up to approx. 1.5×10^{14} [molecules] cm^{-2} $year^{-1}$) and in the Middle East (up to approx. 6.2×10^{13} [molecules] cm^{-2} $year^{-1}$). Negative slopes occur less often and with lower statistic significance. Examples are some European regions (approx. -1.7×10^{14} [molecules] cm^{-2} $year^{-1}$, see also Fig. 2), the east of USA (approx. -1.19×10^{14} [molecules] cm^{-2} $year^{-1}$) and Japan (approx. -1.15×10^{14} [molecules] cm^{-2} $year^{-1}$).

The determined linear trends are in reasonable qualitative agreement with those of other studies (Richter et al., 2005, van der A et al., 2008), although using a slightly different observational periods. Quantitatively, we find significant differences, especially for absolute trends, but also for relative trends. Also some qualitative deviations are found, which are probably related to the different periods of time considered.

4.3 Weekly cycle

The significance of the weekly cycle changes on much smaller spatial scales than it is the case for the annual cycle (Fig. 3). In particular we notice high significances in densely settled and highly industrialized regions. A closer look confirms that many significant points in the global map coincide with big cities.

In figure 6 the weekday with minimum NO_2 TVCD is shown. In the USA, the minima occur mostly on Sunday, when traffic and industrial activity is reduced. The same is true for most regions in Europe and Japan. In cities of the Middle East, the minimum day is on Friday, in Israel the according to the Islamic culture. We can even point out, that the Jewish Sabbath on Saturday in Israel is detected as a significant minimum during the week. No weekend effect could be detected in the big anthropogenic sources of China and South Africa. These findings agree very well with results of former publications (Beirle et al., 2003).

It is interesting to take a closer look on the dependence of the day of the minimum NO_2 TVCD in the plume of strong anthropogenic sources with a strong weekly cycle as in Europe (see Fig. 8). The original Sunday minimum in Western Europe moves eastwards with the dominating west winds. Accordingly the minimum in east Poland occurs on Monday, in the Ukraine on Tuesday, and in Western Russia on Wednesday. This gives an impression about the extent of the influence of NO_x emitted (mainly) in Western Europe. We recognize that the lifetime is long enough to follow this minimum in the plume during a time of four days. Here it should be noted that such long lifetime can be expected only in the winter months.

When applying this model, we obtain information about the temporal behaviour of sources, but also about the area influenced by a source that shows a characteristic temporal behaviour. Such results might be important input for model simulations of the source strengths. The GAM can in particular give a first estimate on the distance up to which sources have to be taken into account for atmospheric models. A more general approach for identifying areas influenced by specific emission sources may be obtained from the wind term in equation (1) discussed in the following.

4.4 Influence of Wind

The wind term increased the accuracy of the model over large areas over the whole globe (Fig 3, bottom). As expected, we find areas with a highly significant contribution of the wind term close to strong continuous sources, such as the East coast of the USA and east Asia, the west coast of European countries and Arabia, and in the environments of point sources like Johannesburg and Hongkong (see also Fig. 1).

We investigate the dependence on the wind direction in more detail for several points located on a circle around the point of maximal mean NO_2 TVCD (Fig. 9). It is obvious that the angle corresponding to the maximum NO_2 TVCD changes according to the position. The highest NO_2 TCVDs are consistently observed from the direction of the strong emission source.

For a larger area of the region of Johannesburg, these directions are shown in figure. 10 (black arrow), together with an indicator of the significance of the wind component (blue color). It is interesting to note that the location of the source corresponds to low significance, as the wind direction is not of importance at this point. In the surrounding of Johannesburg the directions of the maximal wind direction form a highly ordered vector field, even for areas with a rather low significance of the wind term. Tracking the directions -- the arrows in figure 10 -- leads to

large continuous “path ways” all of which leading to the Johannesburg region, and indicating those regions where the central emitter is the major source for non-local NO_2. In the Johannesburg region these zone of wind-related transportation extending in particular over sea, in western and eastern direction and up to more than 1000km. Similar dependencies on the wind-related transport and characteristic emitting point sources in the center could be found for Hong-Kong, Los Angeles, Ar Riyad (Saudi Arabia), Jakarta, although not as sharp as for Johannesburg.

An example for an extended emitting source of NO_2 is western Europe (Fig. 11). High significance is found for areas like the North Sea and North-West France/South-East England which are located close to the main industrial areas of western Europe. For the regions of the main emission sources e.g. in Benelux/Germany and in the Po valley, the wind component is not significant (compare also Fig. 2, Milano). Here the observed NO_2 is dominated by local (constant) sources. It should be noted that the wind directions for maximum observed NO_2 TVCD do not necessarily indicate the directions of the sources contributing the most to the observed NO_2.

Overall, for large areas -- in particular in vicinity to the major industrial areas in the northern hemisphere -- the use of the wind component increased the prediction accuracy significantly (Fig 3). With the correlation between wind and observed NO_2 resulting from a local transport of the trace gas, this model extension may help to uncouple the signal from transport and local generation.

Hence, a more accurate model also helps to get a clearer signal from the other effects.

5 Conclusions

We successfully applied generalized additive models (GAM) to global satellite observations of tropospheric NO_2 (i.e., NO_2 TVCD) from 1996 to 2001. Since GAM does not require regularly sampled data (as it is the case for Fourier analysis), it can be easily applied to satellite observations, which usually contain gaps (e.g. caused by clouds). Thus, in contrast to previous studies, which are based on monthly mean values, our results are based on daily satellite observations.

In this study, we could detect a number of features of the temporal behaviour of the time series of the global tropospheric NO_2 distribution. Annual cycles could be mainly attributed to natural sources or variations of the atmospheric lifetime. Significant linear trends could be found in industrialized regions. Clear weekly cycles appeared in urban areas indicating anthropogenic sources. The location of extremes during the cycles (months of maximal NO_2 TVCD or days of minimal NO_2 TVCD) gave additional insight in the kind of sources or transport processes. These results were in general agreement with former studies.

The non-parametric GAM also allowed to include more complex components like e.g. the wind fields. Including the wind direction from ECMWF data in the model, we could investigate transport processes of plumes of isolated point sources and polluted regions. The wind component was found to be of high importance wherever strong sources border on regions free of permanent sources, like oceans. It was also possible to identify possible pathways of atmospheric pollution and to determine the extent of areas influenced by strong NO_2 emission sources. Such information is important for the correct description of emission sources in atmospheric models.

Our study was limited with respect to several aspects, which should be improved in future studies. The spatial resolution and coverage as well as the temporal sampling of the GOME observations is rather coarse; also the effects of changing sensitivity close to the surface and the influence of clouds on the satellite observations were addressed in a rather simplified way. In the future, increasing satellite data sets with improved spatio-temporal coverage, higher spatial resolution and improved cloud correction will become available. Using such data sets will allow much more detailed studies, taking into account e.g. also the wind speed, vertical wind profiles or additional quantities like temperature and precipitation. Here generalized additive models will provide ideal means for a joint, explorative analysis of observational data

from multiple sources, allowing to access information of complex spatio-temporal pattern easily and to visualize them at a global level.

Acknowledgements

We acknowledge ESA for providing the GOME-spectra. Furthermore, we want to thank ECMWF for permitting access to the ECMWF archives. Bjoern Menze acknowledges support by the German National Academy of Sciences Leopoldina.

References

Aldrin, M. and Haff, I. H.: Generalised additive modelling of air pollution, traffic volume and meteorology, Atmos. Environ., 39(11), 2145–2155, 2005.

Beirle, S., Platt, U., Wenig, M., and Wagner, T.: Weekly cycle of NO2 by GOME measurements: a signature of anthropogenic sources, Atmos. Chem. Phys., 3, 2225–2232, 2003, http://www.atmos-chem-phys.net/3/2225/2003/.

Beirle, S.: Estimating source strengths and lifetime of Nitrogen Oxides from satellite data, PhD thesis, Ruperto-Carola University of Heidelberg, Germany, 2004.

Beirle, S., Platt, U., Wenig, M., and Wagner, T.: NOx production by lightning estimated with GOME, Adv. Space Res., 793–797, 2004.

Boersma, K. F., Eskes, H. J., and Brinksma, E. J.: Error analysis for tropospheric NO2 retrieval from space, J. Geophys. Res., 109, D04311, doi:10.1029/2003JD003962, 2004.

Bovensmann, H., Burrows, J. P., Buchwitz, M. et al.: SCIAMACHY: Mission Objectives and Measurement Modes, J. Atmos. Sci., 56(2), 127–150, 1999.

Brillinger, D.: An application of statistics to meteorology: estimation of motion, in: Festschrift for Lucien Le Cam, edited by: Pollard, D. and Yang, G., Springer, New York, 1994.

Burrows, J. P., Weber, M., Buchwitz, M., et al.: The Global Ozone Monitoring Experiment (GOME): Mission concept and first results, J. Atmos. Sci., 56, 151–175, 1999.

Craven, P. and Wahba, G.: Smoothing noisy data with spline functions, Numer. Math., 31, 377–403, 1979.

Dominici, F., McDermott, A., S. L. Zeger, et al.: On the Use of Generalized Additive Models in Time-Series Studies of Air Pollution and Health, Am. J. Epidemiol., 156(3), 193–203, 2002.

Elsayed, N. M.: Toxicity of nitrogen dioxide: an introduction, Toxicology, 89(3), 161–74, 1994.

ESA: Global Ozone Monitoring Experiment (GOME), Users Manual, ESA Publications Devision, SP-1182, edited by: Bednarz, F., ISBN: 92-9092-327, 1995.

Grzegorski, M.,Wenig, M., Platt, U., Stammes, P., Fournier, N., andWagner, T.: The Heidelberg iterative cloud retrieval utilities (HICRU) and its application to GOME data, Atmos. Chem. Phys., 6, 4461–4476, 2006, http://www.atmos-chem-phys.net/6/4461/2006/.

Hastie, T. J. and Tibshirani, R. J.: Generalized Additive Models, Statistical Science, 1(3), 297–318, 1986.

Hastie, T. J. and Tibshirani, R. J.: Generalized Additive Models, Chapman & Hall/CRC, 1990.

Jacob, D. J.: Introduction to Atmospheric Chemistry, Princeton University Press, 1999.

Jaegle, L., Martin, R. V., Chance, K., et al.: Satellite mapping of rain-induced nitric oxide emissions from soils, J. Geophys. Res., 109, D21310, doi:10.1029/2004JD004787, 2004.

Kallberg, P., Simmons, A., Uppala, S., and Fuentes, M.: ECMWF: The ERA-40 Archive, ERA-40 Project Report Series No. 17, 2004.

Kim, J. and Hong, J.: A GAM for Daily Ozone Concentration in Seoul, Key Eng. Mat., 277–279, 497–502, 2005.

Leue, C., Wenig, M., Wagner, T., Klimm, O., Platt, U., and J¨ahne, B.: Quantitative analysis of NOx emissions from GOME satellite image sequences, J. Geophys. Res., 106(D6), 5493–5505, 2001.

Martin, R. V., Chance, K., Jacob, D. J., et al.: An improved retrieval of tropospheric nitrogen dioxide from GOME, J. Geophys. Res., 107(D20), 4437, doi:10.1029/2001JD001027, 2002.

McCullagh, P. and Nelder, J. A.: Generalized Linear Models, London: Chapman and Hall, 1989.

Olivier et al.: Global air emission inventories for anthropogenic sources of NOx, NH3 and N2O in 1990, Environ. Pollut., 102, 135–148, 1990.

Platt, U.: Differential optical absorption spectroscopy (DOAS), In: Sigrist, M., editor, Air Monitoring by Spectrometric Techniques, 27–84, John Wiley, New York, 1994.

Richter, A. and Burrows, J. P.: Tropospheric NO2 from GOME Measurements, Adv. Space Res., 29(11), 1673–1683, 2002.

Richter, A., Burrows, J. P., N¨uß, H., Granier, C., and Niemeier, U.: Increase in tropospheric

nitrogen dioxide over China observed from space, Nature, 437(7055), 129–132, 2005.

Seinfeld, J. H. and Pandis, S. N.: Atmospheric Chemistry and Physics, John Wiley and Sons, 1997.

Smith, R. L., Davis, J. M., and Speckman, P.: Human health effects of environmental pollution in the atmosphere, In: Barnett V, Stein A, Turkman F, eds. Statistics in the environment 4: statistical aspects of health and the environment, 91–115, Chichester, United Kingdom: John Wiley & Sons Ltd, citeseer.ist.psu.edu/rl99human.html, 1999.

Solomon, S., Schmeltekopf, A. L., and Sanders, R. W.: On the interpretation of zenith sky absorption measurements, J. Geophys. Res., 92, 8311–8319, 1987.

Stige, L. C., Stave, J., Chan, K.-S., Ciannelli, L., Pettorelli, N., Glantz, M., Herren, H. R., and Stenseth, N. C.: The effect of climate variation on agro-pastoral production in Africa, Proceedings of the National Academy of Sciences, PNAS, 103(9), 2006.

Stohl, A., Huntrieser, H., Richter, A., Beirle, S., Cooper, O. R., Eckhardt, S., Forster, C., James, P., Spichtinger, N., Wenig, M., Wagner, T., Burrows, J. P., and Platt, U.: Rapid intercontinental air pollution transport associated with a meteorological bomb, Atmos. Chem. Phys., 3, 969–985, 2003, http://www.atmos-chem-phys.net/3/969/2003/.

Toutenburg, H. and Heumann, C.: Induktive Statistik, Eine Einf ¨uhrung mit R und SPSS Reihe, Springer-Lehrbuch, 2008.

Uno, I., Ohara, T., and Wakamatsu, S.: Analysis of wintertime NO2 pollution in the Tokyo Metropolitan area, Atmos. Environ., 30(5), 703–713(11), 1996.

van der A, R. J., Peters, D. H. M. U.,, Eskes, Boersma, K. F., Van Roozendael, M., De Smedt, I., and Kelder, H. M.: Detection of the trend and seasonal variation in tropospheric NO2 over China, J. Geophys. Res., 111, D12317, doi:10.1029/2005JD006594 2006.

van der A, R. J., Eskes, H. J., Boersma, K. F., van Noije, T. P. C., Van Roozendael, M., De Smedt, I., Peters, D. H. M. U., Kuenen, J. J. P., and Meijer, E. W.: Identification of NO2 sources and their trends from space using seasonal variability analyses, J. Geophys. Res., 113, doi:10.1029/2007JD009021, 2008.

Velders, G. J. M., Granier, C., Portmann, R. W., Pfeilsticker, K., Wenig, M., Wagner, T., Platt, U., Richter, A., and Burrows, J. P.: Global tropospheric NO2 column distributions: Comparing three-dimensional model calculations with GOME measurements, J. Geophys. Res., 106(D12), 12643–12660, 2001.

Wagner, T., Beirle, S., Deutschmann, T., Eigemeier, E., Frankenberg, C., Grzegorski, M., Liu, C., Marbach, T., Platt, U., and Penning de Vries, M.: Monitoring of atmospheric trace gases, clouds, aerosols and surface properties from UV/vis/NIR satellite instruments, J. Opt. A: Pure Appl. Opt., 10, 104019, doi:10.1088/1464-4258/10/10/104019, 2008.

Wakamatsu, S., Uno, I., and Ohara, T.: Springtime Photochemical Air Pollution in Osaka: Field Observation, J. Appl. Meteorol., 37, 1100–1106, 1998.

Wenig, M., Spichtinger, N., Stohl, A., Held, G., Beirle, S., Wagner, T., J¨ahne, B., and Platt,

U.: Intercontinental transport of nitrogen oxide pollution plumes, Atmos. Chem. Phys., 3,

387–393, 2003, http://www.atmos-chem-phys.net/3/387/2003/.

Wood, S. N.: Generalized Additive Models: An Introduction with R, Chapman & Hall/CRC,

Taylor & Francis Group, 2006.

World Health Organization, Health Aspects of Air. Pollution with Particulate Matter, Ozone and Nitrogen Dioxide. Report on a WHO Working Group, 13–15 January 2003, Bonn, Germany.

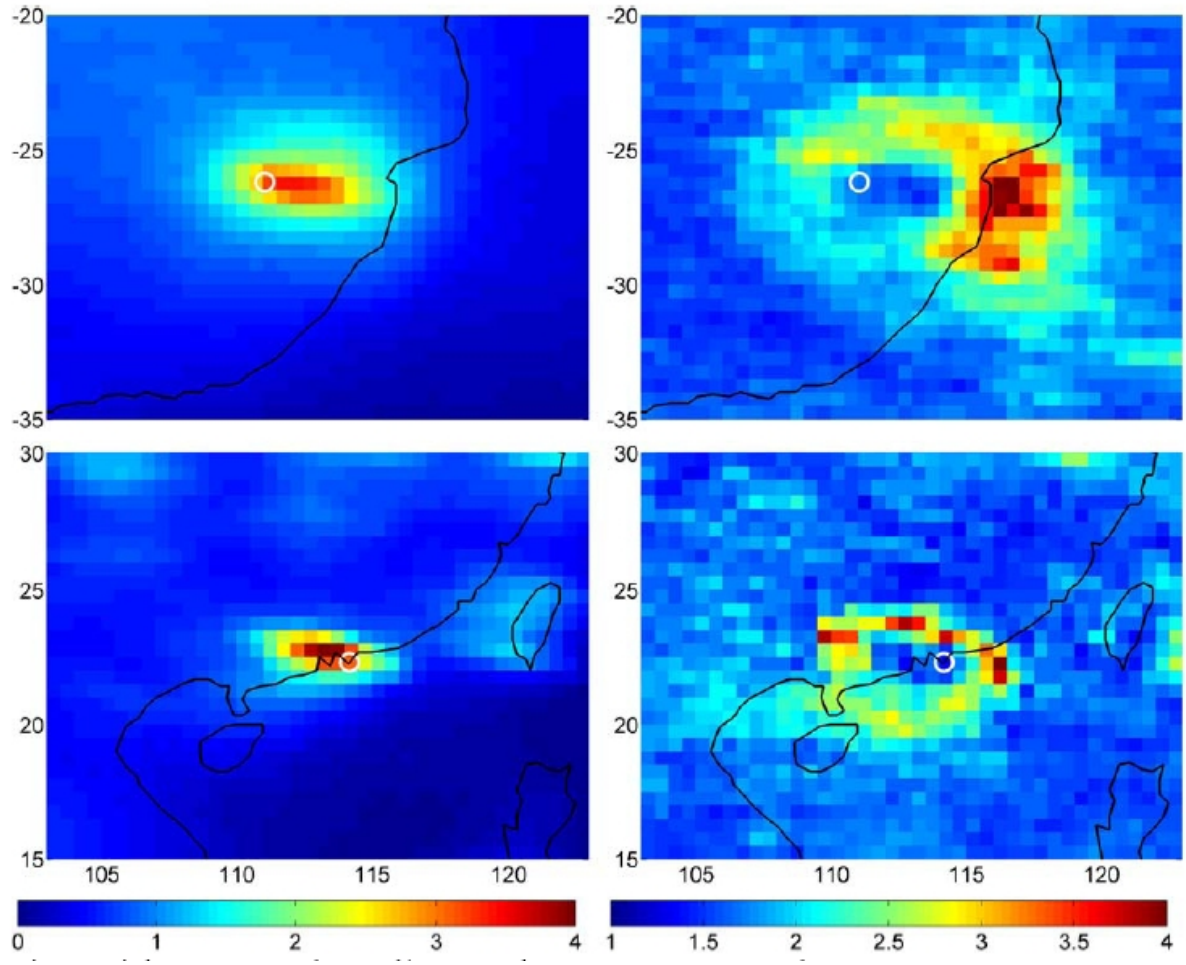

Figure 1. Left: Mean tropospheric vertical column density (TVCD) of NO_2 (10^{15} molec/cm^2) around Johannesburg (top) and Hong Kong (bottom). Right: Ratio of standard deviation over MAD (median absolute deviance) for the respective regions. The high ratios between the two variability measures around the local minimum of the sources are consequences of transport processes. High values indicate that the transport is dominated by relatively few, though large events.

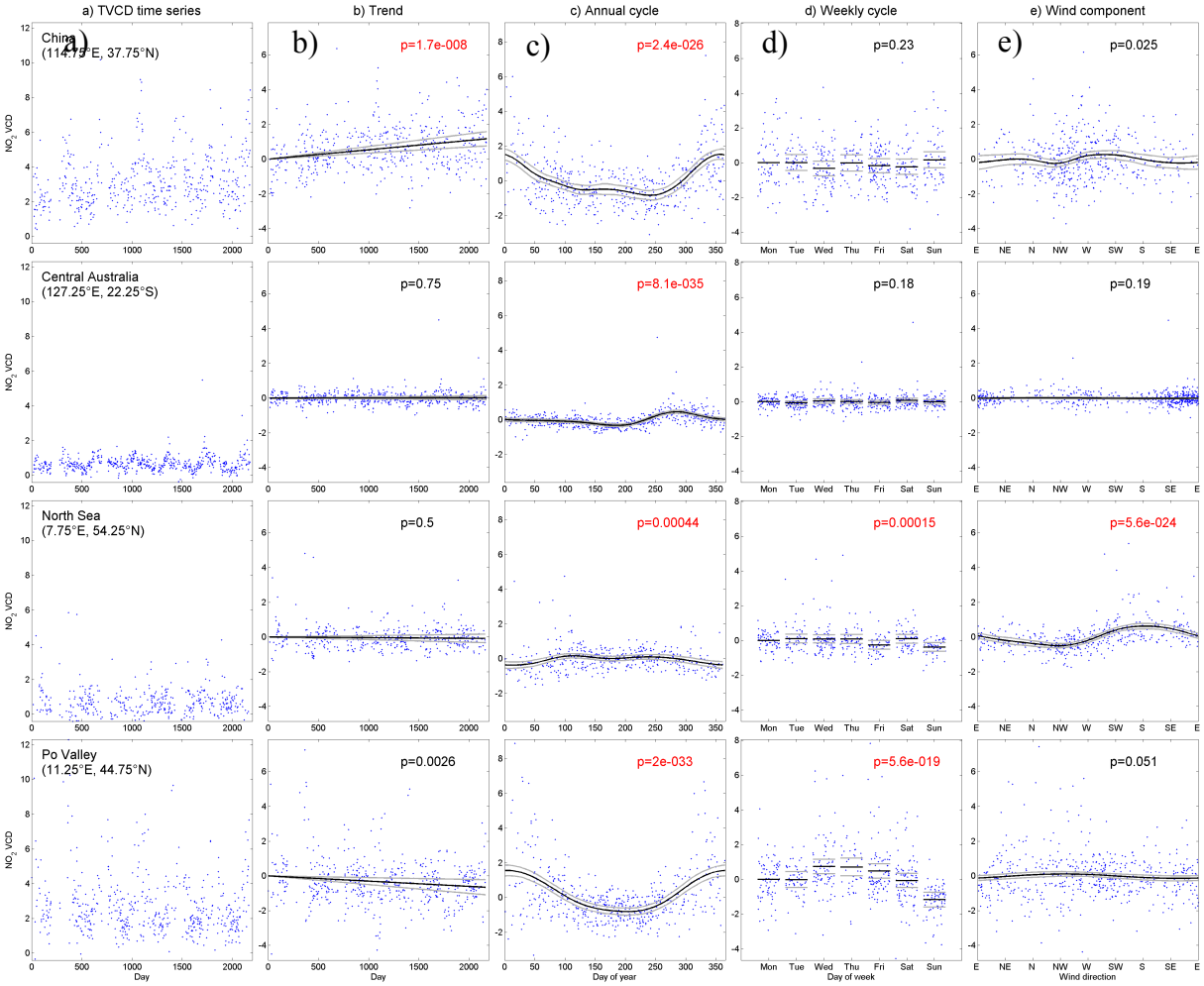

Figure 2. Examples of the GAM components for China, Central Australia, the North Sea, and the Po Valley. a) The original TVCD time series. b) The trend component. c) The Annual cycle. d) The weekly cycle. e) The wind component. The dots in b)-e) illustrate the individual measurements corrected for all other GAM components. The numbers give the GAM p-values, indicating the significance of the respective component. p-values below 1°/oo are considered as significant and marked in red.

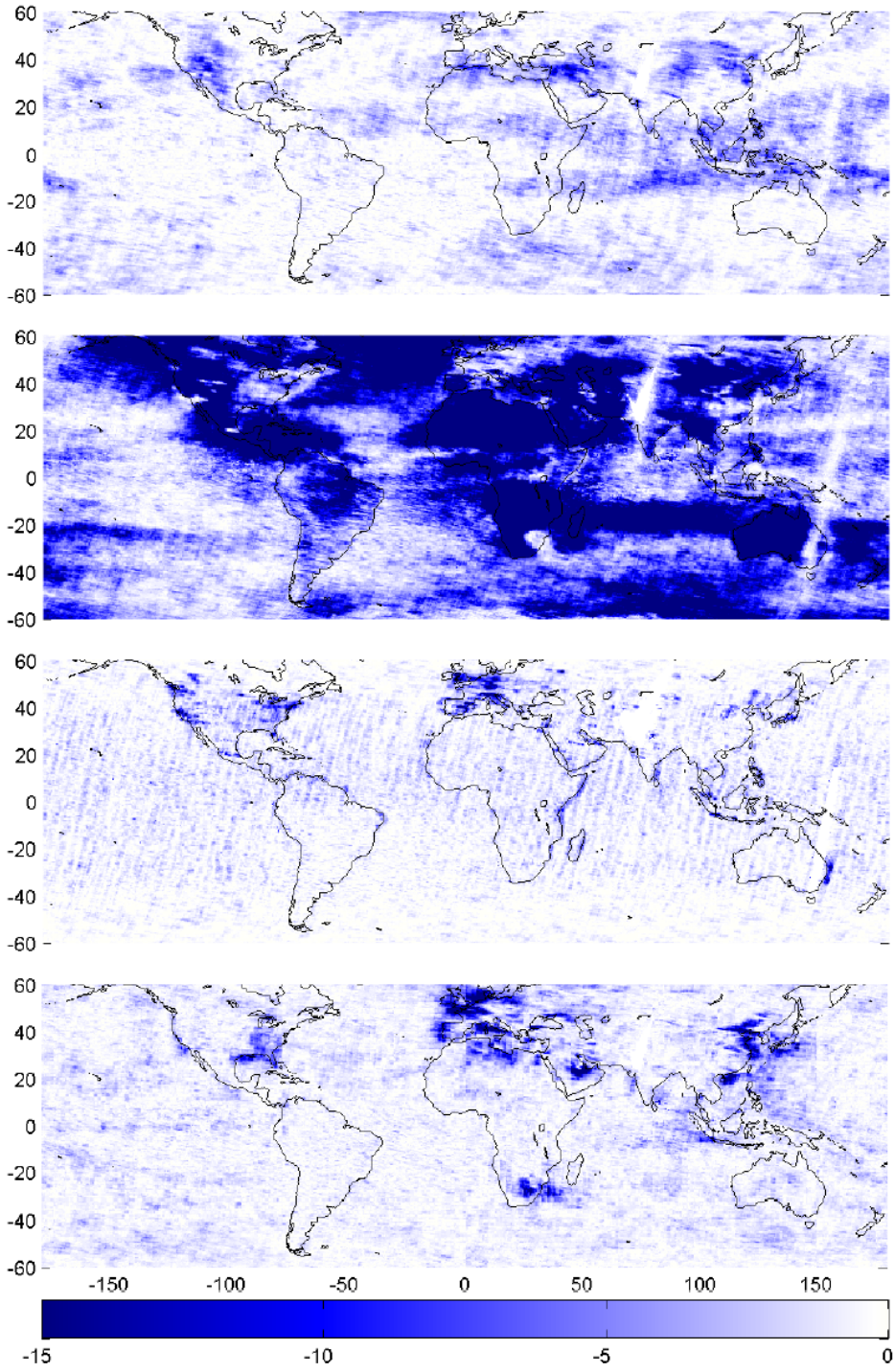

Figure 3. The significance (log10 of the p-value) of the different GAM terms, i.e. trend, annual cycle, weekly cycle, and wind component (from top). Dark blue areas are affected significantly by the respective term.

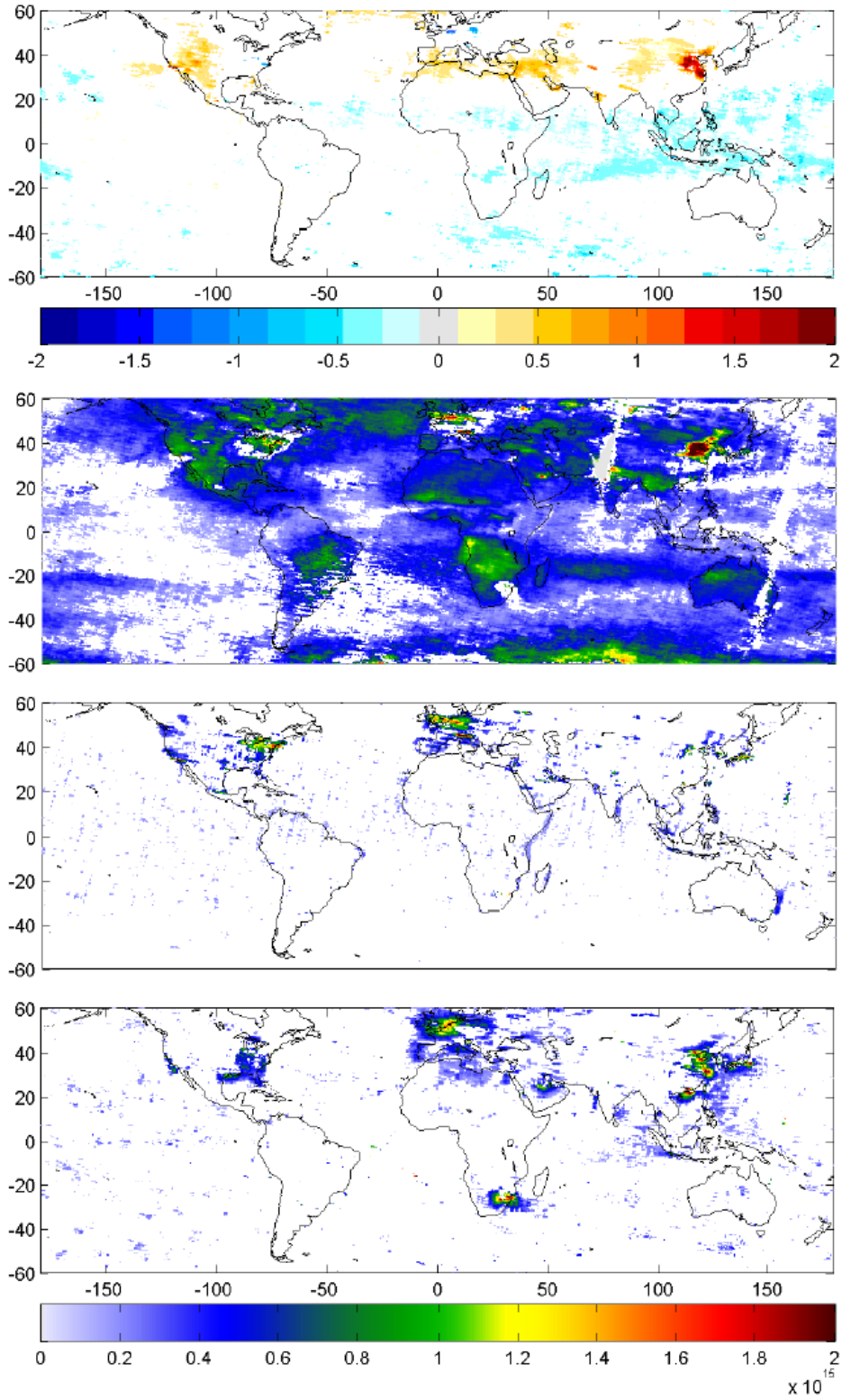

Figure 4. The strength of the different GAM terms. a) Absolute trend in 10^{14} molec/cm^2 per year. b) Amplitude of the annual cycle (peak to peak in molec/cm^2). c) Amplitude of the weekly cycle (peak to peak in molec/cm^2). d) Amplitude of the wind component (peak to peak in molec/cm^2).

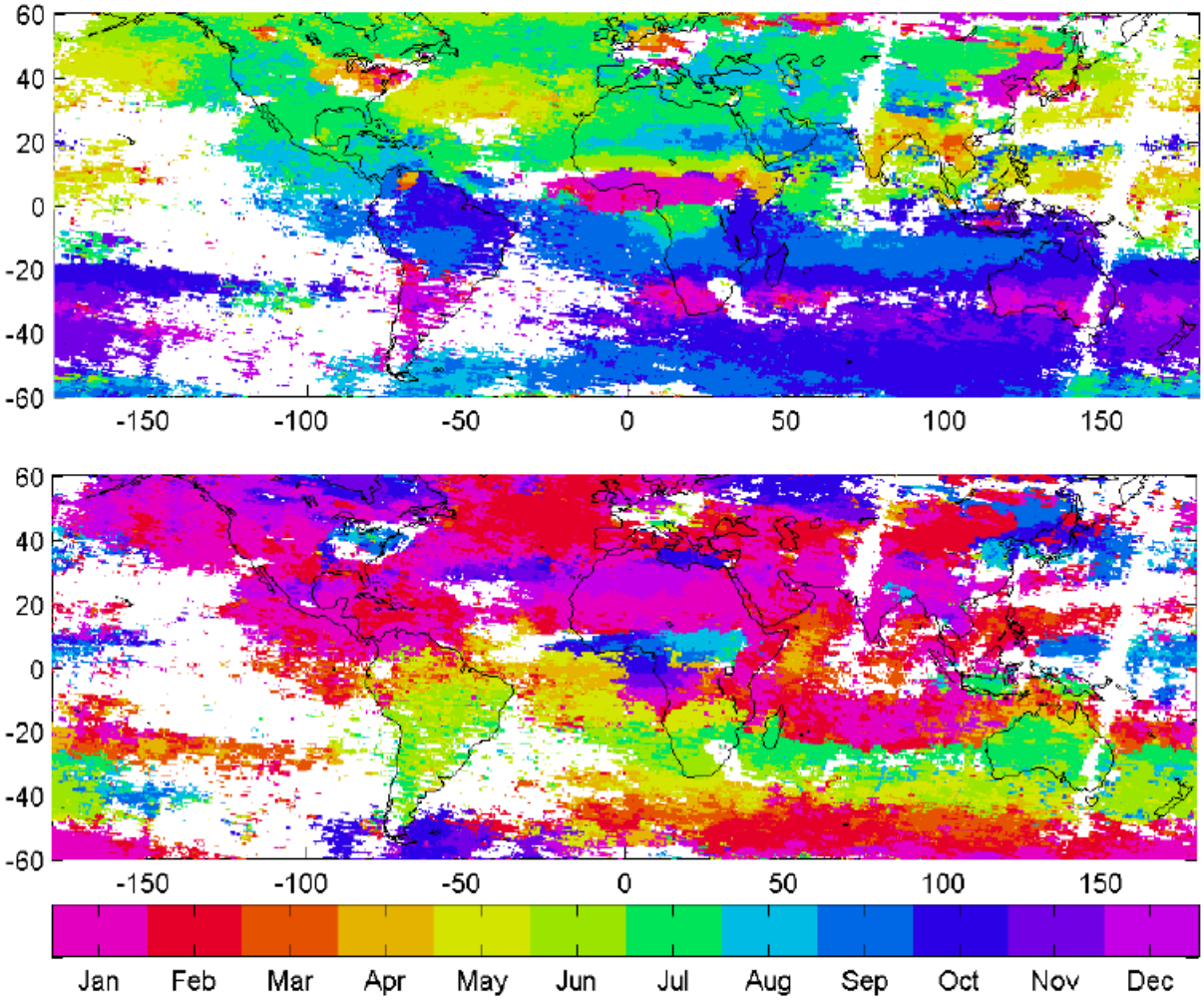

Figure 5. Month with (a) maximum and (b) minimum TVCD.

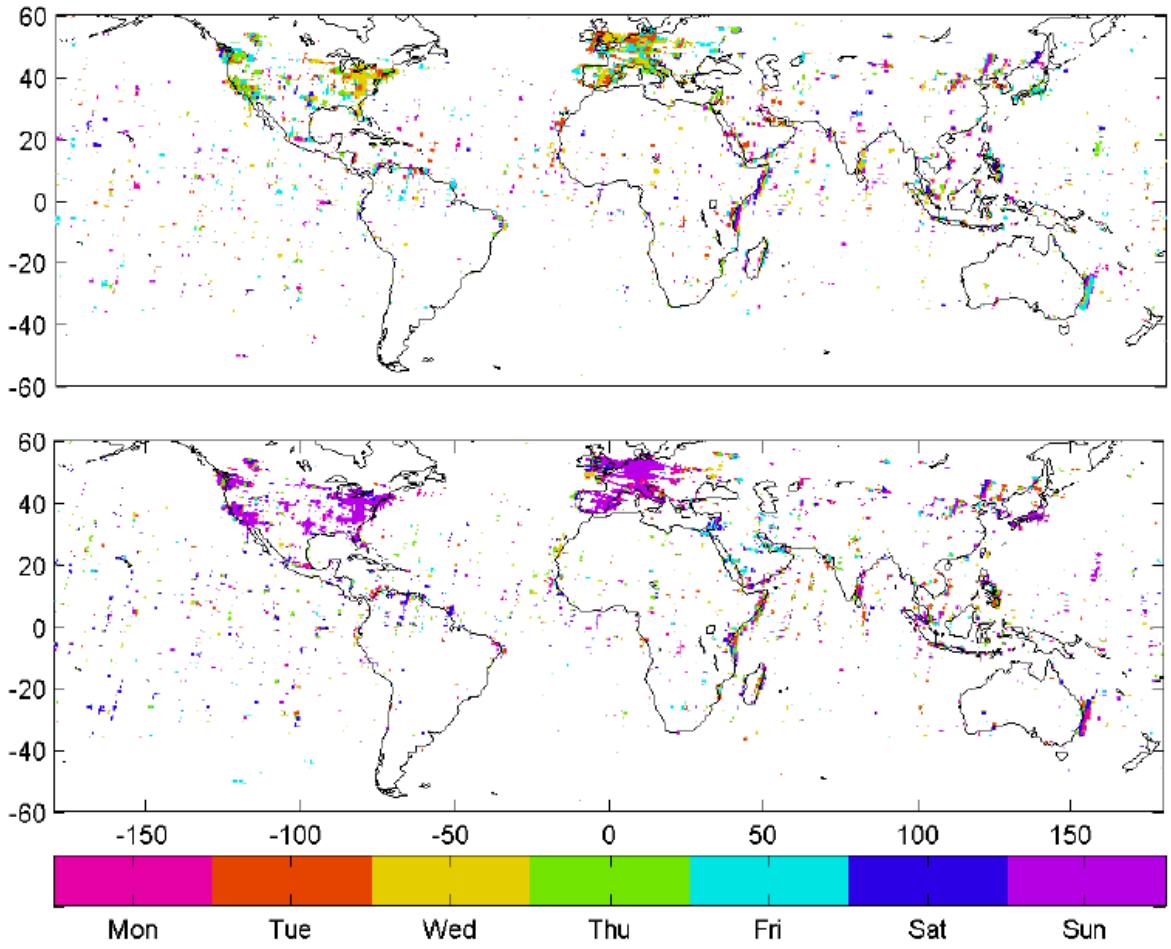

Figure 6. Day of week with (a) maximum and (b) minimum TVCD.

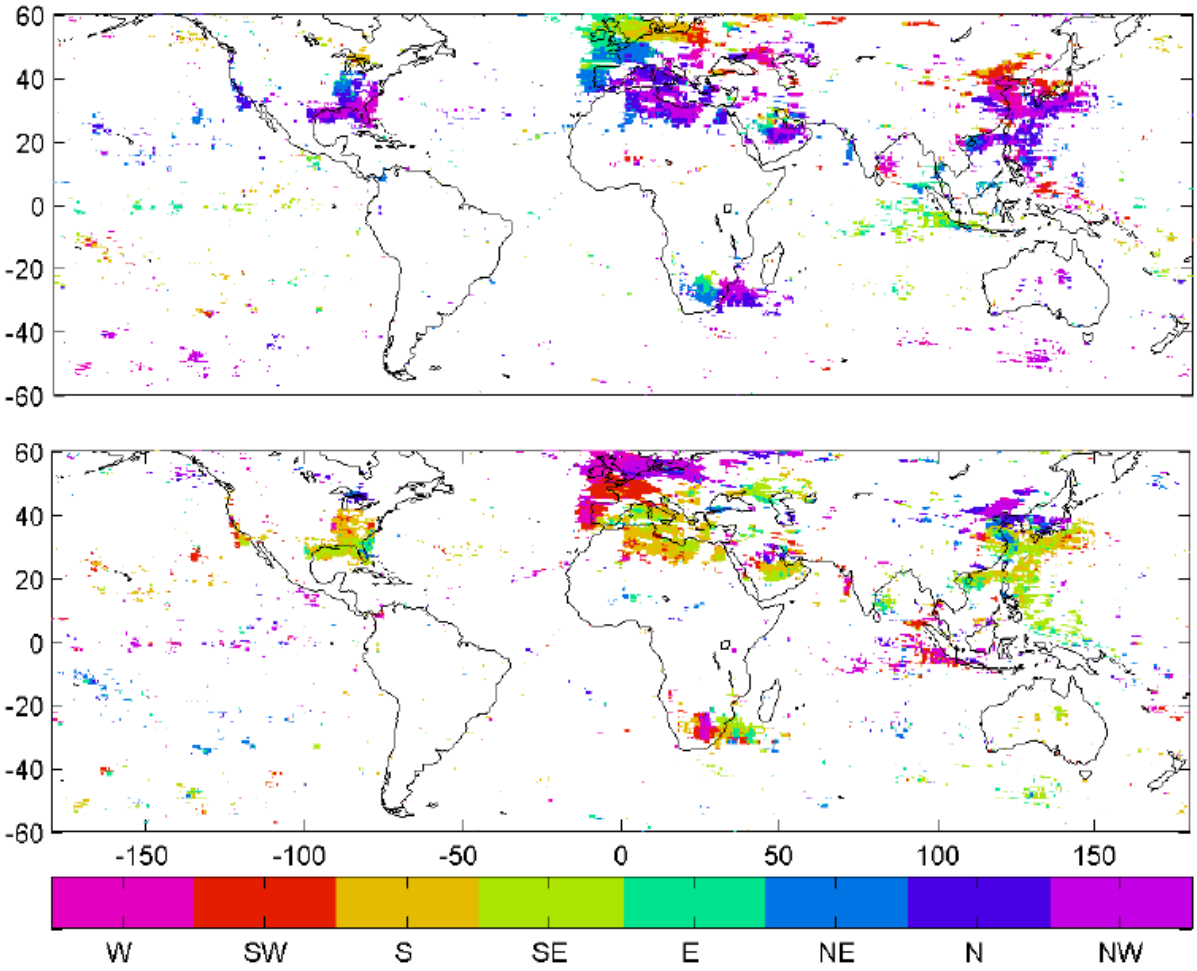

Figure 7. Wind direction with (a) maximum and (b) minimum TVCD.

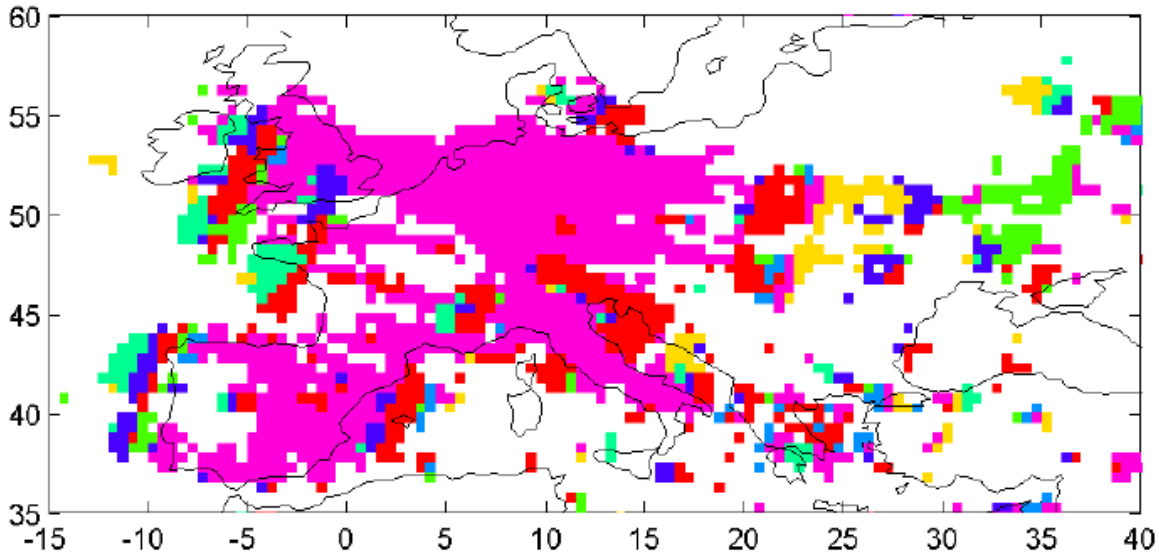

Figure 8. Day of week with minimum TVCD (see Figure 6b) for Europe. Over most regions, the minimum occurs on Sunday. In eastern Europe the minimum is shifted to the beginning of the week indicating the transport of the temporal emission patterns of the strong western NO_x sources with the dominating westerly winds. Only data of p-values less than 0.001 are shown. Colors coded as in figure 6.

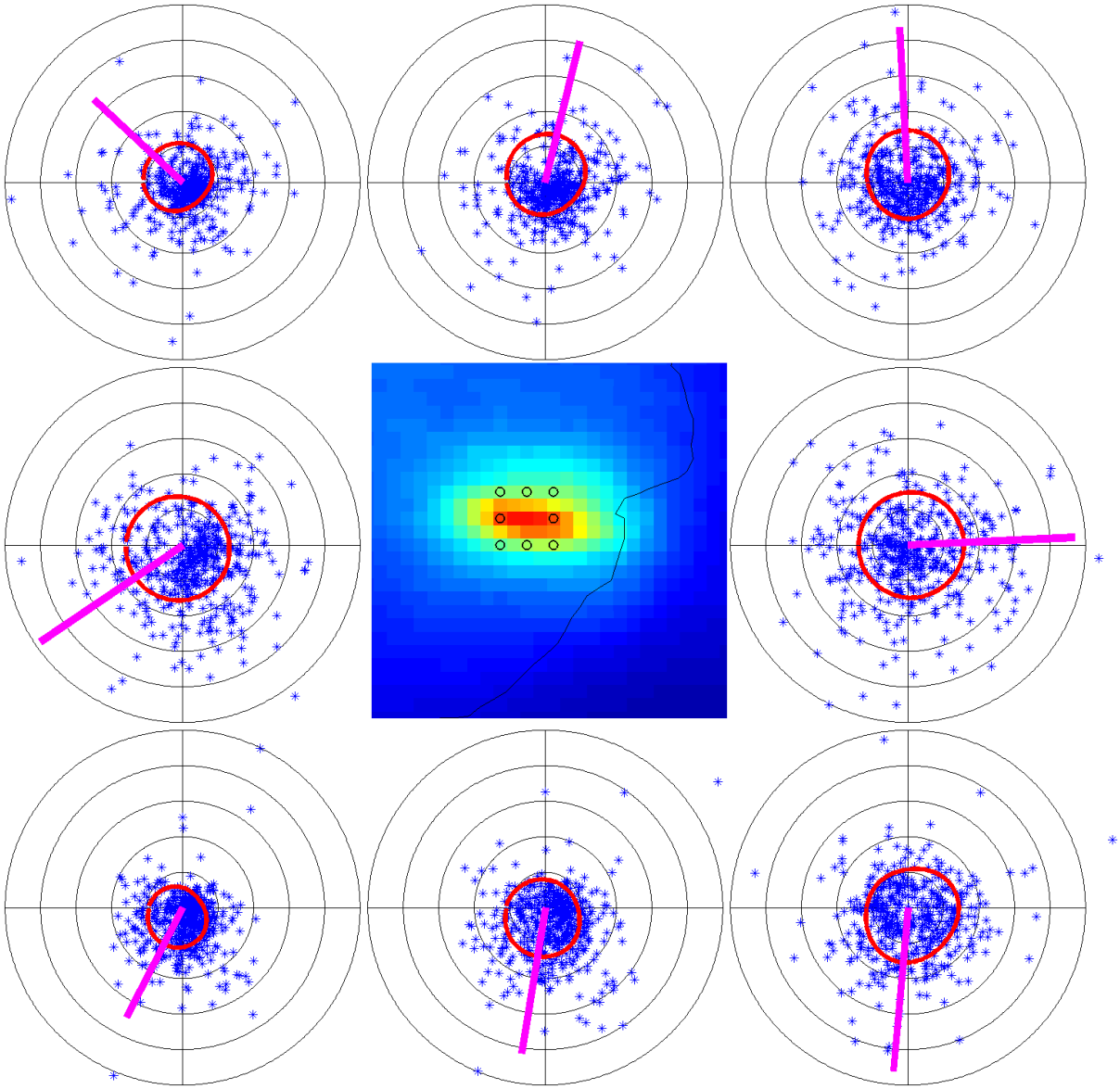

Figure 9. The dependencies of the NO_2 TVCD (red circle indicates the fitted spline) on the wind direction for 8 points around Johannesburg (see image in the center). The wind direction of maximum NO_2 TVCD (pink pointer indicate the direction of the air flux) changes accordingly to the position relative to the center.

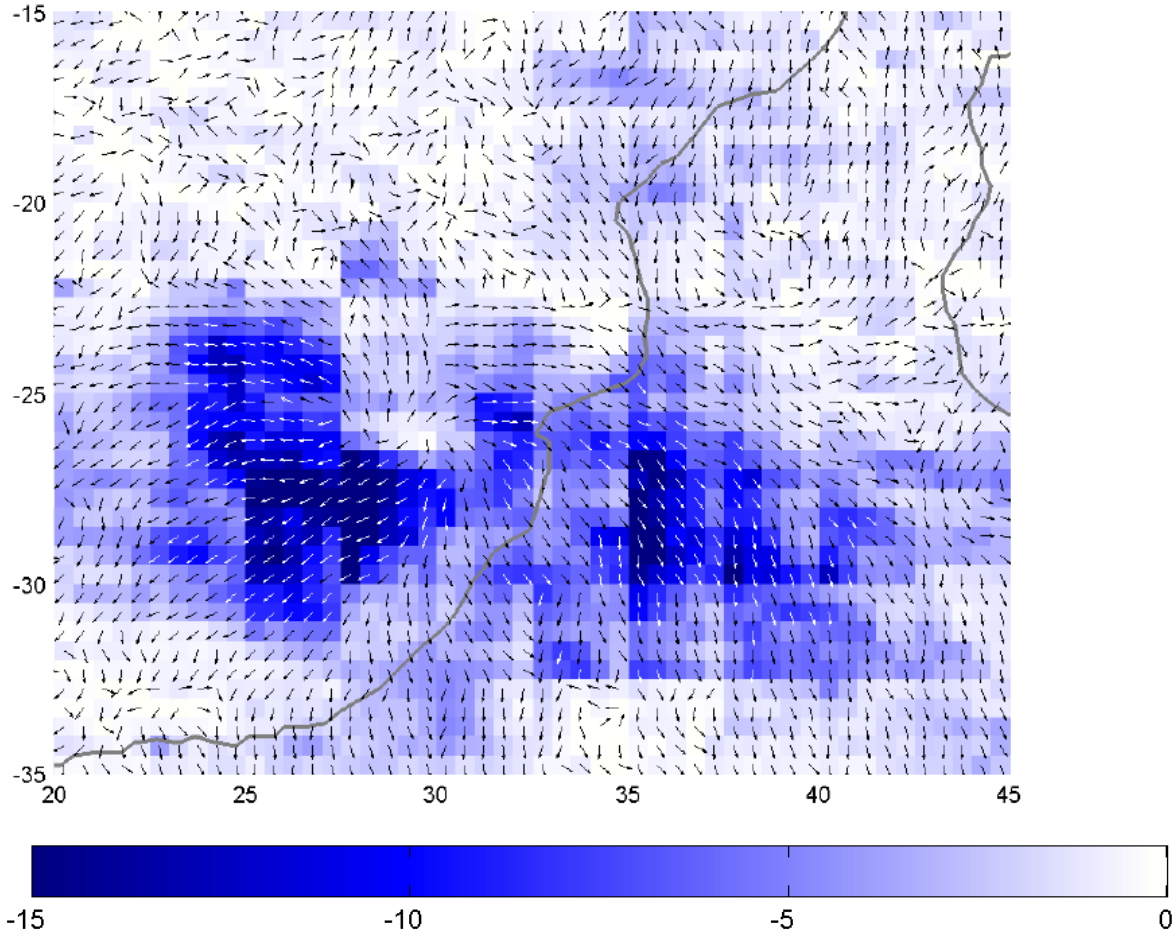

Figure 10. Wind direction of maximum TVCD as quiver-plot (compare Fig. 7a) for the region around Johannesburg, South Africa. Also the significance as in figure 3d is shown (strength of the blue color).

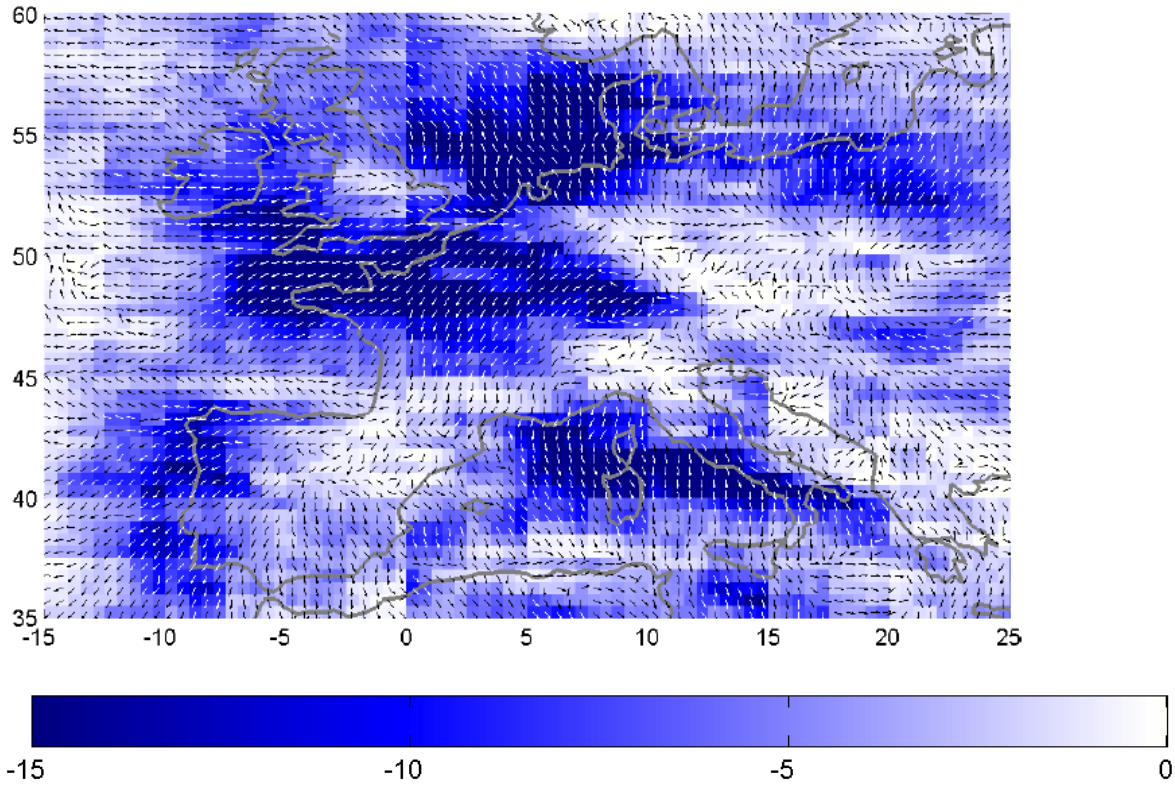

Figure 11. Wind direction of maximum TVCD as quiver-plot (compare Fig. 7a) over Europe. Also the significance as in Fig. 3d is shown (strength of the blue color).